Combustion and Flame 258 (2023) 113054

Contents lists available at ScienceDirect

Combustion and Flame

journal homepage: www.elsevier.com/locate/combustflame

Computational diagnostics for flame acceleration and transition to detonation in a hydrogen/air mixture

S. Lai [a], S. Tang [a], C. Xu [b], N. Sekularac [c], X. Fang [d,e,*]

[a] School of Aeronautics and Astronautics, Shanghai Jiao Tong University (SJTU), Shanghai, China
[b] Transportation and Power Systems Division, Argonne National Laboratory, Lemont, IL 60439, USA
[c] CERFACS, 42 Avenue Gaspard Coriolis, Toulouse, 31057, France
[d] Department of Engineering Science, University of Oxford, Oxford, OX1 3PJ, UK
[e] Department of Mechanical & Manufacturing Engineering, Schulich School of Engineering, University of Calgary, Calgary, T2L 1Y6, Canada

ARTICLE INFO

Article history:
Received 25 April 2023
Revised 28 August 2023
Accepted 29 August 2023

Keywords:
Numerical simulation
Turbulent combustion
Deflagration to detonation transition
Chemical explosive mode analysis

ABSTRACT

A new computational diagnostic method for pressure-induced compressibility is proposed by projecting its local contribution to the chemical explosive mode (CEM) in the chemical explosive mode analysis (CEMA) framework. The new method is validated for the study of detonation development during the deflagration-to-detonation transition (DDT) process. The flame characteristics are identified through the quantification of individual CEM contributions of chemical reaction, diffusion, and pressure-induced compressibility. Numerical simulations are performed to investigate the DDT processes in a stoichiometric hydrogen-air mixture. A Godunov algorithm, fifth-order in space, and third-order in time are used to solve the fully compressible Navier-Stokes equations on a dynamically adapting mesh. A single-step, calibrated chemical diffusive model (CDM) described by Arrhenius kinetics is used for energy release and conservation between the fuel and the product. The new diagnostic method is first applied to one-dimensional (1D) canonical flame configurations followed by two-dimensional (2D) simulations of DDT in an obstructed channel where different detonation initiation scenarios are examined using the new CEMA projection formulation. Detailed examinations of the idealized configuration of detonation initiation through shock focusing mechanism at a flame front are also studied using the new formulation. A comparison of the currently proposed CEMA projection and the original formulation by the authors suggests that including the pressure-induced compressibility is essential for the use of CEMA in DDT process. The results also show that the new formulation of CEMA projection can successively capture the detonation initiation through either a gradient mechanism or a direct initiation mechanism, and therefore can be used as an effective local analytical tool for the computational diagnostics of detonation initiation in a DDT process. It was found that detonation development is characterized by a strong contribution of chemistry role to the CEM which is pivotal to the initiation of detonation. The role of compressibility is found enhanced at the edge of the detonation front where diffusion was found to have minimal effects on detonation development.

Novelty and Significance Statement: A new computational diagnostic method for pressure-induced compressibility is proposed by projecting its local contribution to the chemical explosive mode (CEM) in the chemical explosive mode analysis (CEMA) framework. The proposed method is tested and validated for the study of detonation development during the deflagration to detonation transition (DDT) process. The new method is found to be an effective local analytical tool for the computational diagnostics of detonation initiation in a DDT process. The proposed method is versatile and can be used on various different platforms which makes this study more impactful.

* Corresponding author.
E-mail address: xiaohang.fang@ucalgary.ca (X. Fang).

https://doi.org/10.1016/j.combustflame.2023.113054

1. Introduction

As a carbon-free fuel, hydrogen is widely considered an important future energy vector [1]. Potential advantageous properties of hydrogen as a fuel include wide flammability limits, high laminar burning velocity, and low ignition energy. However, these listed advantages might also be considered disadvantages from a safety perspective. The hazardous potential of hydrogen-air mixtures has been studied in the literature extensively by assuming perfect mixing of fuel and oxidant. Studies have suggested that reactive hydrogen and air mixtures may detonate if ignited in confined areas [2,3]. Under favorable circumstances, small flames or sparks in hydrogen-oxygen mixtures can also accelerate and undergo deflagration-to-detonation transition (DDT), posing serious safety risks [4,5]. DDT, as a result of flame acceleration, is an important topic for a broad range of scientific and engineering problems of interest. However, the fundamental mechanisms by which small flames/sparks can lead to detonations have not been fully understood by combustion theory [6]. This is due, in part, to the fact that DDT is a highly rapid and nonlinear phenomenon that is stochastic and dependent on the details of the confining geometry and the fuel and oxidizer mixture. The physics of the flame acceleration and DDT processes also involve a number of intricate phenomena, including flow instabilities, shock waves, boundary layers, turbulence, and detonation initiation.

For applications such as detonation-based propulsion systems [7,8], a deeper understanding of the detonation initialization mechanism is necessary. Detonation initiations can be achieved in different ways, among which the most straightforward one, as described by Xiao and Oran [4], is through direct initiation, where a detonation is created directly without first producing a deflagration [9,10]. As detailed in the literature, direct initiation is possible when a significant amount of external energy is added to a reactive mixture at a timescale smaller than the acoustic timescale [11,12]. Alternatively, the initiation of detonation can be part of the response of a reactive gas to an intense localized explosion during deflagration. For this scenario, the local background conditions favoring detonation are created through shock waves created by an accelerating flame. This process to form detonation is known as DDT [6]. In DDT process, detonation is often produced through a reactivity-gradient mechanism, initiated by a “hot spot”. This gradient mechanism was first simulated by Zeldovich et al. [13]. The basic idea is that a spontaneous reaction wave can propagate through a reactive material if there is a spatial gradient in chemical induction time and a detonation forms when the spontaneous wave decelerates to D_{CJ} [6]. This phenomenon was later observed in experiments conducted by Lee et al. [14] and was referred to as the SWACER (Shock Wave Amplification by Coherent Energy Release) mechanism. For the SWACER mechanism, the reaction front would transit into a detonation for an appropriate gradient of the free radical concentration and the evolution occurs through the amplification of shock waves. More recently, Xiao and Oran detailed the shock-focusing detonation initiation mechanism at the flame front, where detonation is found to be initiated through multi-shock collision in an energetic gas [4].

The above-mentioned studies have provided significant physical insights into detonation initiation mechanisms by resolving the flame front thickness and the half-reaction thickness where a significant amount of computational cells are allocated. For most of the listed studies, conventional diagnostic methods based on individual scalars, such as temperature, concentrations of selected species, or some form of conditional scalars (e.g., progress variable and mixture fraction), have been used to identify detonation initiation. The use of such diagnostic methods might become particularly challenging for processing DDT data where a vast range of timescales and lengthscales exist within the system. The diagnostic methods based on individual scalars also typically require semi-empirical criteria (e.g. local pressure threshold [15]) that need to be adjusted for different flame types and conditions, limiting their application to specific flame configurations. With the increase in computational cells, the need for three-dimensional simulations, incorporating detailed chemistry, and developing novel post-processing tools capable of extracting key information from the dataset might be necessary. Previous studies have also suggested DDT might be a spatially and temporally stochastic process even when the flow is subjected to minimal fluctuations of initial conditions [16,17]. Therefore, it is of great interest to develop a universal data diagnostics tool for delineating DDT mechanisms while conventional diagnostic methods may fail.

Among others, eigenanalysis-based methods have been used to resolve complex physiochemical couplings between flows and chemical kinetics in incompressible turbulent reactive flows [18,19]. In particular, the chemical explosive mode (CEM) analysis (CEMA) method has been developed to identify key flame features relevant to explosive modes in high-fidelity reactive flow simulations. First developed by Lu et al. [20], CEMA analyses the dominant eigenmodes of the chemical Jacobian, highlighting the reactive mixtures relevant to critical combustion events such as autoignition, flame propagation, and extinction. Xu et al. [21] further advanced the CEMA theory by proposing to project the chemical and non-chemical (e.g., diffusion) source terms in the governing equations for reactive flows to the CEM. Different flame propagation modes were thereafter identified by the new criteria highlighting the role of the competition between projected reaction/diffusion source terms. The proposed CEMA approach has been used in various reacting flows, including premixed laminar and turbulent flames, spray flames, supersonic and detonative flames [3,7,8,21–24]. However, the compressibility effects caused by the density variation of the local fluid particle, which may play important roles in supersonic flames and DDT processes, are not accounted for in these studies using CEMA. Recently, Wu et al. proposed a conservative representation of CEMA (CCEMA) for flame diagnostics, attempting to account for the compressibility effect in compressible reactive flows [25]. The CCEMA method was applied to analyze the flame stabilization mechanisms in the Burrows-Kurkov supersonic flames, where chemical reactions are found to control the flame kernel formation, indicating that autoignition governs the flame stabilization. However, the density variation effects identified by CCEMA may or may not be related to pressure change, and thus its application to complex flame scenarios, such as DDT where both deflagration and detonation-induced density variations are present, becomes challenging. It is also worth noting that the eigenmode in CCEMA depends on the flow field, and, thus, is not a local chemical property - a key feature of the CEM in the original CEMA formulation. As suggested by various studies, shock focusing can be a critical mechanism for the initiation of DDT, making it essential to consider pressure-induced compressibility in computational diagnostics for DDT.

In this study, a novel CEMA implementation catering to pressure-induced compressibility for DDT processes has been formulated and tested. The contributions of the chemical reaction, diffusion, and compressibility projecting to the direction of the CEM are detailed to systematically investigate the detonation initiation mechanisms from DDT processes. The validity of the proposed method is first demonstrated in one-dimensional (1D) subsonic hydrogen-air premixed flames and the Chapman-Jouguet detonation. The new method is further applied to the two-dimensional (2D) simulation data of hydrogen-air deflagration to detonation and idealized detonation initiation cases where the capability of the method in capturing different detonation initiation mechanisms is examined.

2. Physical models and numerical methods

2.1. Governing equations

In this paper, governing equations for the conservation of mass, momentum, energy, and species for an unsteady, fully compressible, chemically reactive flow are solved [6,26]:

$$\frac{\partial \rho}{\partial t} + \nabla \cdot (\rho \mathbf{U}) = 0 \tag{1}$$

$$\frac{\partial (\rho \mathbf{U})}{\partial t} + \nabla \cdot (\rho \mathbf{U}\mathbf{U}) + \nabla p = \nabla \cdot \hat{\boldsymbol{\tau}} \tag{2}$$

$$\frac{\partial (\rho E)}{\partial t} + \nabla \cdot ((\rho E + p)\mathbf{U}) = \nabla \cdot (\mathbf{U} \cdot \hat{\boldsymbol{\tau}}) + \nabla \cdot (K \nabla T) - \rho q \dot{\omega} \tag{3}$$

$$\frac{\partial (\rho Y)}{\partial t} + \nabla \cdot (\rho Y \mathbf{U}) + \nabla \cdot (\rho D \nabla Y) = \rho \dot{\omega} \tag{4}$$

where ρ, $\mathbf{U}$, p, and T represent the density, velocity, pressure, and temperature of the gas, respectively. E is the energy density, $\dot{\omega}$ is the chemical reaction rate, q is the chemical energy release, Y is the mass fraction of the reactant, K is the thermal conductivity, and D is the mass diffusivity.

The gas equation of state follows the ideal gas law,

$$p = \frac{\rho R T}{M} \tag{5}$$

where R is the universal gas constant, and M is the molecular weight.

The viscous stress tensor is defined as

$$\hat{\tau} = \rho \nu ((\nabla \mathbf{U}) - (\nabla \mathbf{U})^T - \frac{2}{3}(\nabla \cdot \mathbf{U})\mathbf{I}) \tag{6}$$

where ν is the kinematic viscosity, $\mathbf{I}$ is the unit tensor, and the superscript T denotes the matrix transposition. The specific energy density E is calculated by

$$E = \frac{p}{(\gamma - 1)\rho} + \frac{1}{2}(\mathbf{U} \cdot \mathbf{U}) \tag{7}$$

where γ is the specific heat ratio.

2.2. The chemical diffusive model

The premixed stoichiometric combustion of hydrogen-air mixture is studied using a calibrated, one-step chemical-diffusive model (CDM) [16] where the reaction rate follows a first-order Arrhenius equation:

$$\dot{\omega} = dY/dt = -A\rho Y \exp(-E_a/RT) \tag{8}$$

where A and E_a represent the pre-exponential factor and the activation energy, respectively. In this model, it is assumed that the kinematic viscosity, diffusion, and heat conduction all depend on the temperature in a comparable way:

$$\nu = \nu_0 \frac{T^{0.7}}{\rho}, \quad D = D_0 \frac{T^{0.7}}{\rho}, \quad \frac{K}{\rho C_p} = \kappa_0 \frac{T^{0.7}}{\rho} \tag{9}$$

The diffusive processes of CDM are characterized by transport constants ν_0, D_0, and κ_0. $C_p = \gamma R/\ M(\gamma - 1)$ is the specific heat at a given pressure, and the temperature exponent 0.7 represents the temperature dependency of these coefficients in the reactive system. The relation between ν_0, D_0, and κ_0 is expressed by three dimensionless parameters, Lewis, Prandtl, and Schmidt numbers:

$$\text{Le} = \frac{K}{\rho C_p D} = \frac{\kappa_0}{D_0}, \quad \text{Pr} = \frac{\rho C_p \nu}{K} = \frac{\nu_0}{\kappa_0}, \text{Sc} = \frac{\nu}{D} = \frac{\nu_0}{D_0} \tag{10}$$

Eqs. (1)-(10) are solved using input values for the chemical and thermophysical parameters for stoichiometric hydrogen-air mixture to reproduce the major properties of the flame in the chemical reaction. Table 1 provides specific input thermal-chemical parameters for the CDM and the output characteristics for combustion waves computed using these parameters. Specifically, the laminar flame thickness χ_l in this table is defined as the distance between the isosurfaces of reactant mass fraction $Y = 0.1$ and $Y = 0.9$. The input values for CDM are carefully calibrated to correctly reproduce the one-dimensional laminar flame properties and Zeldovich-von Neumann-Döring (ZND) detonation structure within a reasonable error range where the values used in this study follow earlier works of Gamezo et al. [16]. The calibration procedure for various chemical diffusive models is concluded and detailed by Lu et al. [27]. While modified input CDM values exist in the literature [28], the values in this study are purposely chosen for the development of the computational diagnostics tools. Previous studies have also revealed the limitations of using one-step chemistry, particularly for capturing the accurate chemical ignition response of the gas [10,29]. More recent studies also highlighted the use of multi-step chemistry or detailed chemistry can be more attractive for the onset prediction of transverse detonations near the critical limit [30]. While the inclusion of multi-step/full chemistry might be essential for certain conditions, the CDM one-step chemistry used in this study was found capable of quantitatively reproducing a wide range of scenarios from slow deflagration, fast deflagration, predetonation, overdriven detonation, stable detonation, and has been widely used to study DDT problems [4].

Table 1
Input model parameters and output combustion wave properties for stoichiometric premixed hydrogen and air initially at 1 atm and 293 K [16].

Parameter	Descriptions	Value
Input		
T_0	Initial temperature	293 K
P_0	Initial pressure	1 atm
ρ_0	Initial density	0.87 kg/m^3
γ	Specific heat ratio	1.17
M	Molecular weight	21 kg/kmol
A	Pre-exponential factor	6.85×10^9 m^3/(kg-s)
E_a	Activation energy	46.37 RT_0
q	Chemical energy release	43.28 RT_0/M
$\kappa_0 = D_0 = \mu_0$	Transport constants	2.9×10^{-6} kg/s-m-K$^{0.7}$
Output		
S_L	Laminar flame speed	2.98 m/s
T_b	Post-flame temperature	7.289 T_0
ρ_b	Post-flame density	0.137 ρ_0
χ_l	Laminar flame thickness	0.35 mm
χ_d	Half-reaction thickness	0.193 mm
D_{CJ}	CJ detonation velocity	1993 m/s
P_{ZND}	Post-shock pressure	31.47 P_0
P_{CJ}	Pressure at CJ point	16.24 P_0
T_{ZND}	Post-shock temperature	3.457 T_0
T_{CJ}	Temperature at CJ point	9.01 T_0
ρ_{ZND}	Post-shock density	9.104 ρ_0
ρ_{CJ}	Density at CJ point	1.902 ρ_0
λ	Detonation cell size	$\sim$ 1–2 cm

2.3. Numerical algorithm

The equations are solved using a fifth-order WENO algorithm with HLLC fluxes for spatial discretization and a third-order Runge-Kutta scheme for time advancement. To improve the resolution in specific areas and save computational cost, an adaptive mesh refinement (AMR) technique has been integrated using the Boxlib library [31,32]. In order to capture the detail of shocks and flames, an AMR refinement criterion consisting of several rules is adopted. First, cells with a reactant mass fraction $0.005 < Y < 0.995$ will be regarded as flame and refined. In addition, increased resolution is triggered based on the change of Y values among the neighboring cells.

To capture shocks, turbulence, and other important flow structures, the spatial variation along the x-axis of pressure is calculated as:

$$\begin{aligned}\delta_0 &= \max(|p_{i,j} - p_{i-1,j}|, |p_{i,j} - p_{i+1,j}|)\\ \delta_1 &= |p_{i+1,j} - p_{i-1,j}|\\ \delta_2 &= |p_{i+2,j} - p_{i-2,j}|\end{aligned} \tag{11}$$

Similar calculations are performed for y direction and two diagonal directions. Then, a cell will be tagged as shock and refined if

$$\alpha_{AMR}\delta_2 <= \quad \delta_1 or \quad \delta_0 > \quad d\,p_{shock} \tag{12}$$

where α_{AMR} and dp_{shock} are parameters to control the refinement tolerance. In particular, $\alpha_{AMR} = 0.9$ and $dp_{shock} = 100$ is adopted in the following simulations. Moreover, an AMR rule based on the maximum error of density for each grid cell, $e_{i,j} = \max\left(\varphi_x, \varphi_y, \varphi_{xy}, \varphi_{yx}\right)$, in x, y, and both diagonals is applied. Specifically, φ_x is calculated as:

$$\varphi_x = \frac{\left|\rho_{i-1,j} - 2\rho_{i,j} + \rho_{i+1,j}\right|}{0.03\left|\rho_{i,j}\right| + \left|\rho_{i+1,j} - \rho_{i-1,j}\right|} \tag{13}$$

Similar calculations are performed for $\varphi_y, \varphi_{xy}, \varphi_{yx}$. In summary, a cell is tagged for refinement based on local gradients in pressure, temperature, and reactant concentration. The current AMR grid resolution has been shown to resolve flames, shocks, boundary layer, and other important flow and chemical structures [6]. Details of the grid size for each case can be found in the results sections.

2.4. Computational flame diagnostic tool

The chemical explosive mode analysis (CEMA) used in this study originated from the work by Lu et al. [20] which is an eigenanalysis for the chemical Jacobian to identify critical combustion events such as autoignition, flame propagation, and extinction in reactive mixtures. The evolution of the chemical source term in a reactive flow system is governed by:

$$\frac{D\boldsymbol{\omega}(\boldsymbol{y})}{Dt} = \boldsymbol{J}_\omega \frac{D\boldsymbol{y}}{Dt} = \boldsymbol{J}_\omega(\boldsymbol{\omega} + \boldsymbol{s}), \boldsymbol{J}_\omega = \frac{\partial \boldsymbol{\omega}}{\partial \boldsymbol{y}} \tag{14}$$

where $\boldsymbol{y}$ is the vector form of dependent variables (e.g. temperature and species concentrations). $\boldsymbol{\omega}$ and $\boldsymbol{s}$ are the chemical source term and the non-chemical source term (e.g., diffusion) associated with the system. A chemical explosive mode (CEM) is identified when the chemical Jacobian ($\boldsymbol{J}_\omega$) has an unstable eigenvalue characterized by a positive real part λ_e with the corresponding left eigenvector denoted by $\boldsymbol{b}_e$. In order to identify different local combustion modes in a detonation cycle, an extended criterion developed by Xu et al. [21] is adapted here, where Eq. 14 is projected to the direction of CEM through $\boldsymbol{b}_e$, giving:

$$\boldsymbol{b}_e \cdot \frac{D\boldsymbol{\omega}(\boldsymbol{y})}{Dt} = \boldsymbol{b}_e \cdot \boldsymbol{J}_\omega(\boldsymbol{\omega} + \boldsymbol{s}) = \lambda_e \boldsymbol{b}_e \cdot (\boldsymbol{\omega} + \boldsymbol{s}) \tag{15}$$

$$\frac{D\phi_\omega}{Dt} = \lambda_e \phi_\omega + \lambda_e \phi_s + \frac{D\boldsymbol{b}_e}{Dt} \cdot \boldsymbol{\omega} \tag{16}$$

where,

$$\phi_\omega = \boldsymbol{b}_e \cdot \boldsymbol{\omega}, \quad \phi_s = \boldsymbol{b}_e \cdot \boldsymbol{s} \tag{17}$$

According to Xu et al. [21], a local combustion mode indicator, α, is further defined as:

$$\alpha = \phi_s/\phi_\omega. \tag{18}$$

Previous studies on incompressible reactive flows have used this definition of α to highlight the relative importance of chemical and diffusive source terms in the ignition process, where different local combustion modes can be identified using the following criterion [21]: (i) $\alpha > 1$: the assisted-ignition mode, where diffusion dominates chemistry and promotes ignition; (ii) $|\alpha| < 1$: the auto-ignition mode, where chemistry plays a dominant role in the ignition with diffusion being less important; (iii) $\alpha < -1$: the local extinction mode, where diffusion dominates chemistry but reverses the ignition process. In order to accommodate the use of such criteria in supersonic or DDT studies, the above criteria were used with conditional variables (e.g. progress variables, Damköhler number) to identify the different regimes of a DDT or detonation process [3,24]. However, the contributions from mixture compressibility to chemical explosive modes were not included in these analyses, which limits the use of such criteria for the study of detonation initiation in a DDT process. As highlighted before, Wu et al. [25] attempted to use a conservative representation of CEMA to analyze the flame stabilization mechanisms. While individual contributions of diffusion, chemistry, and compressibility for the flame stabilization mechanisms are highlighted by Wu et al., no specific criterion is established for the study of detonation initiation. Furthermore, this study, distinct from Wu et al.'s study, isolates the contributions from pressure-induced compressibility splitting the non-chemical source terms $\boldsymbol{s}$ into diffusion ($\boldsymbol{s_d}$) and compression ($\boldsymbol{s_p}$) terms, that is:

$$\boldsymbol{s} = \boldsymbol{s_d} + \boldsymbol{s_p} \tag{19}$$

and the projections of the two terms to CEM are,

$$\phi_{s_d} = \boldsymbol{b}_e \cdot \boldsymbol{s_d}, \quad \phi_{s_p} = \boldsymbol{b}_e \cdot \boldsymbol{s_p} \tag{20}$$

In order to obtain $\boldsymbol{s_p}$, several steps are needed. First, governing equations of mass, energy, and species can be rewritten as:

$$\frac{\partial u_j}{\partial x_j} = -\frac{1}{\rho}\frac{D\rho}{Dt} \tag{21}$$

$$\begin{aligned}&\rho c_p\left(\tfrac{\partial T}{\partial t} + u_j \tfrac{\partial T}{\partial x_j}\right) = -\textstyle\sum_{k=1}^{n_s} h_k \dot{\omega}_k W_k + \tfrac{Dp}{Dt} + \tfrac{\partial}{\partial x_j}\left(\lambda \tfrac{\partial T}{\partial x_j}\right)\\ &-\left(\textstyle\sum_{k=1}^{N} \rho c_{p,k} Y_k V_{k,j}\right)\tfrac{\partial T}{\partial x_j}\end{aligned} \tag{22}$$

$$\rho\left(\frac{\partial Y_k}{\partial t} + u_j \frac{\partial Y_k}{\partial x_j}\right) = \dot{\omega}_k W_k - \frac{\partial\left(\rho Y_k V_{k,j}\right)}{\partial x_j} \tag{23}$$

Taking the time derivative of the equation of the state of an ideal gas Eq. 5 we can get:

$$\frac{1}{p}\frac{Dp}{Dt} = \frac{1}{\rho}\frac{D\rho}{Dt} + \frac{1}{T}\frac{DT}{Dt} + \sum_{k=1}^{n_s}\frac{\bar{W}}{W_k}\frac{DY_k}{Dt} \tag{24}$$

From Eq. 24, Eq. 21 can be rewritten as:

$$\frac{\partial u_j}{\partial x_j} = -\frac{1}{\rho}\frac{D\rho}{Dt} = \frac{1}{T}\frac{DT}{Dt} + \sum_{k=1}^{n_s}\frac{\bar{W}}{W_k}\frac{DY_k}{Dt} - \frac{1}{p}\frac{Dp}{Dt} \tag{25}$$

Substituting Eq. 22 and Eq. 23 into Eq. 25:

$$\begin{aligned}\frac{\partial u_j}{\partial x_j} &= \frac{1}{\rho c_p T}\Bigg(-\sum_{k=1}^{n_s} h_k \dot{\omega}_k W_k + \frac{Dp}{Dt} + \frac{\partial}{\partial x_j}\left(\lambda \frac{\partial T}{\partial x_j}\right) - \left(\sum_{k=1}^{N} \rho c_{p,k} Y_k V_{k,j}\right)\frac{\partial T}{\partial x_j}\Bigg)\\ &\quad + \frac{1}{\rho}\sum_{k=1}^{n_s}\frac{\bar{W}}{W_k}\left(\dot{\omega}_k W_k - \frac{\partial\left(\rho Y_k V_{k,j}\right)}{\partial x_j}\right) - \frac{1}{p}\frac{Dp}{Dt}\\ &= \frac{1}{\rho c_p T}\left(-\sum_{k=1}^{n_s} h_k \dot{\omega}_k W_k + \frac{\partial}{\partial x_j}\left(\lambda \frac{\partial T}{\partial x_j}\right) - \left(\sum_{k=1}^{N} \rho c_{p,k} Y_k V_{k,j}\right)\frac{\partial T}{\partial x_j}\right)\\ &\quad + \frac{1}{\rho}\sum_{k=1}^{n_s}\frac{\bar{W}}{W_k}\left(\dot{\omega}_k W_k - \frac{\partial\left(\rho Y_k V_{k,j}\right)}{\partial x_j}\right) + \left(\frac{p}{\rho c_p T} - 1\right)\frac{1}{p}\frac{Dp}{Dt}\end{aligned} \tag{26}$$

The first two terms of the right-hand side can be defined as the thermal divergence term, Q_T, giving the following:

$$\frac{\partial u_j}{\partial x_j} = Q_T - \frac{1}{\gamma p}\frac{Dp}{Dt} \tag{27}$$

$$\frac{Dp}{Dt} = \gamma p\left(Q_T - \frac{\partial u_j}{\partial x_j}\right) \tag{28}$$

Finally, the $\boldsymbol{s_p}$ term is defined as $\frac{Dp}{Dt}/\rho c_p$, which can be projected to the direction of CEM through the left eigenvector of the chemical Jacobian ($\boldsymbol{b_e}$). The evolution of the projected chemical reaction can therefore be expressed as:

$$\frac{D\phi_\omega}{Dt} = \lambda_e\phi_\omega + \lambda_e\phi_{s_d} + \lambda_e\phi_{s_p} + \frac{D\boldsymbol{b}_e}{Dt}\cdot\boldsymbol{\omega} \tag{29}$$

The last term of Eq. 29 represents the nonlinear effect induced by the rotation of left eigenvectors. The attractiveness of such an approach is that it can be easily implemented where the focus can be on the competition between diffusion, chemistry, and pressure-induced compressibility on detonation initiation. It is also worth noting that the current formulation is written in the Lagrangian form, to be consistent with the CEMA formulation in the previous work of Lu et al. [20] and Xu et al. [21]. However, when adopting these terms in the Eulerian CFD solver used in this work, the material derivative is converted and expressed in terms of Eulerian quantities. As a result, the proposed method works as a local post-processing tool and is compatible with the Eulerian framework.

3. Results and discussion

3.1. One-dimensional flame

In order to validate the proposed new CEMA method, three canonical one-dimensional premixed hydrogen-air flames are simulated to investigate the roles of different physiochemical processes for the CEMs under DDT conditions. The three representative one-dimensional flames chosen for the DDT process include laminar flame propagation, fast flame deflagrations, and Chapman-Jouguet (CJ) detonation, where CEMA analyses are performed for each case for validation. As suggested by earlier experimental and numerical works for DDT in a long smooth walled tube, the onset of spontaneous detonation takes place in a deflagration when it accelerates to some maximum velocity of the order of about half the CJ detonation speed [33]. Therefore, the fast deflagration flame considered in this study corresponds to initiation conditions without spontaneous detonations. The deflagration is represented by the post-shock laminar flames where initiation conditions are obtained from the shock detonation (SD) toolbox corresponding to the frozen state behind a shock, whose Mach number corresponds to 40% CJ speed. Similar approaches can be found in the literature where post-shock laminar flames are found to be representative of the chemical structure of the deflagration behind the shock in the fast flame regime [24,34,35]. The fast deflagration state obtained from the SD toolbox (with elevated temperature and pressure) is then adopted in a 1D domain with no shock and a hot spot located at one end of the domain. The hot spot is composed of an equilibrated mixture at constant enthalpy and pressure, similar to the authors' previous work [3]. For brevity, the canonical post-shock deflagrations are referred to as post-shock laminar flames in the following section. All 1D simulations listed above are performed by the in-house unsteady detonation code. Details of the initial conditions of the four 1D flames can be found in Table 2.

Table 2
Initial conditions of 1D simulations .

Initial conditions				
Symbol	Descriptions	Laminar	40% D_{CJ}	ZND
T_0	Initial temperature	293 K	483 K	293 K
P	Initial pressure	1 atm	4.3 atm	1 atm

Profiles of diffusion, chemistry, and compressibility to the CEMs from the laminar freely propagating premixed flame and post-shock laminar flame (40% D_{CJ}) are shown in Fig. 1. It is worth noting that only explosive mixtures identified by a positive λ_e are shown with projected contributions. Perhaps not surprisingly for both scenarios, it is found that ϕ_{s_d} is larger than ϕ_ω at a lower temperature where a crossover point of ϕ_{s_d} and ϕ_ω can be found near the temperature of 1000 K. When the chemistry becomes dominant in the CEM as the temperature becomes higher, the fresh mixture is found to ignite in the preheat zone suggesting that the flame is a canonical deflagration wave. The reaction zone thickness is found significantly shorter for the fast deflagration flame. As expected, no compressibility contribution can be found in these two flames. These results correspond well with previous studies both experimentally and numerically, where in the case of a deflagration, the reaction front will propagate via diffusive transport compared to autoignition across the leading shock front for a detonation [33].

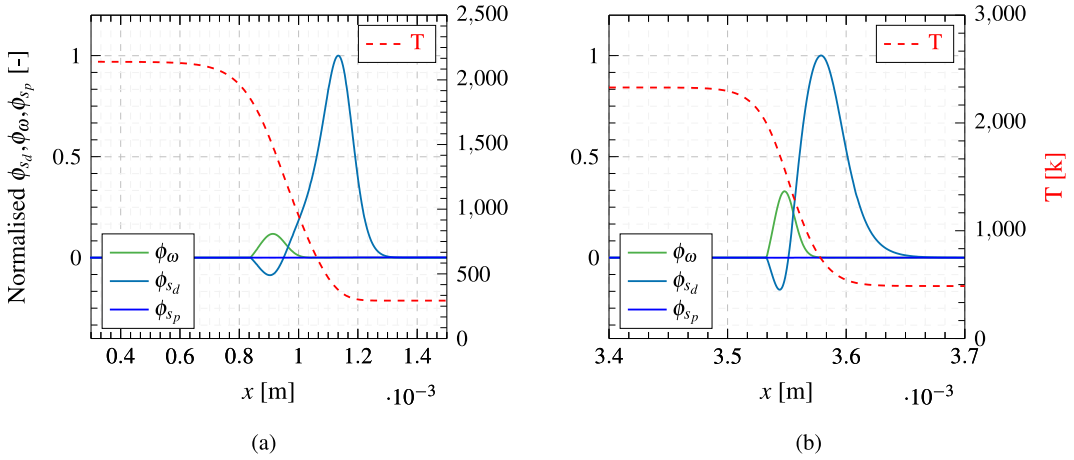

Fig. 1. Profiles of normalized ϕ_{s_d}, ϕ_ω and ϕ_{s_p} and temperature for a) 1-D freely propagating laminar premixed hydrogen-air flame b) laminar flame at post-shock conditions for a shock traveling at 0.4 D_{CJ}.

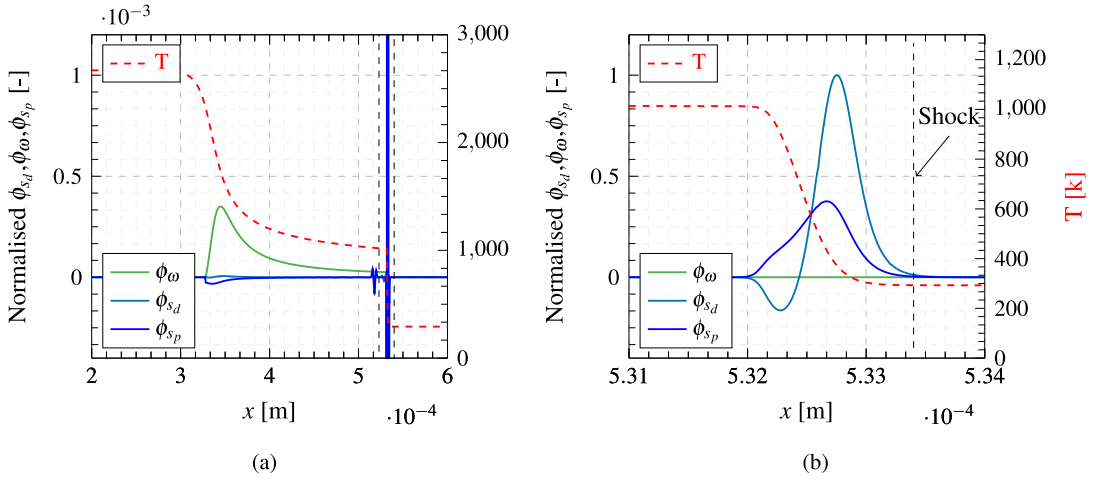

Fig. 2. Profiles of ϕ_{s_d}, ϕ_ω, ϕ_{s_p} and temperature profiles for a CJ detonation a) full profile b) zoomed-in view of induction period indicated by dashed vertical lines in Fig 2 (a).

Figure 2 shows the profiles of diffusion, chemistry, and compressibility projection to the CEMs for the ZND solutions of a hydrogen-air CJ detonation. Figure 2(b) focuses on the region near the shock front covering the induction zone. The mixture downstream of the shock wave (shown in Fig. 2(a)) is chemically explosive dominated by ϕ_ω, indicating that it is autoignitive after shock wave compression, and the compressibility is dominant among the nonchemical effects. However, for this region, the major difference noticed is that the compressibility contributions are negative, which indicates that this could inhibit the ignition process. The finding downstream of the shock wave using the current CEMA criteria is consistent with the study conducted by Wu et al. using conservative CEMA [25], with the distinction that the compressibility contribution in the present study is solely induced by pressure. Perhaps more relevant to the purpose of this study are the findings near the induction zone. From classical theory, deflagration can be distinguished from detonation by differences in the ignition mechanisms, categorizing diffusion (for deflagration) and autoignition (for detonation). The transition can be characterized by a switchover from diffusion to autoignition via shock compression. This can be clearly demonstrated in Fig. 2(b) where during the induction period, a cross-over is found between diffusion (ϕ_{s_d}) and compressibility (ϕ_{s_p}) contributions, which then leads to a dominant chemistry contribution shown in the reaction zone (Fig. 2(a)). However, whether this compressibility contribution comes from the adiabatic compression of the reactants by the precursor shock or by precursor compression waves is not clear from the current analysis, which warrants further investigation. It is worth mentioning that at the very beginning of the reaction zone, there are fluctuations in pressure projection (ϕ_{s_p}) that are induced by a small numerical perturbation in pressure for the ZND calculation. This small value is then enlarged through the calculation of ϕ_{s_p}. The real contribution of chemical, diffusion, and compressibility to the CEM in this region is negligible as the CEM is at a nearly frozen state.

The new CEMA analysis for 1D flames suggests that the proposed method is able to identify the relative contributions of different physical processes to the CEMs under various physical processes relevant to DDT. Particularly, it is found that the current analysis can clearly distinguish the differences between deflagration and shock-induced detonation, which can be used to identify the detonation initiation in multi-dimensional high-fidelity DDT simulations, particularly for shock-focusing detonation mechanism. Therefore, the new method is then introduced to analyze the DDT scenario in an obstructed channel.

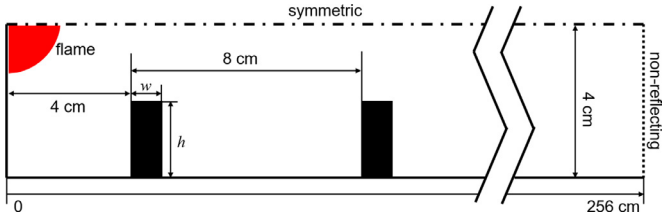

Fig. 3. Computational setup for 2D calculations. Obstacles of size $h \times w$ are evenly spaced along the channel wall.

3.2. DDT In channels with obstacles

In this section, numerical simulations on a canonical configuration [16,26,36,37], namely an obstructed channel filled with energetic gas, are carried out. The proposed CEMA is then applied to analyze the local chemical kinetics during the DDT ignition process, with particular emphasis on the contribution of pressure-induced compressibility. The two-dimensional channel geometry is shown in Fig. 3. The computational area is the bottom half of the channel, and the upper boundary is considered a symmetry plane. The left and bottom boundaries are modeled as solid walls, where no-slip, adiabatic boundary conditions are used, and the right end is an open outlet. The channel length (L) and width (D) are 256 cm and 8 cm, respectively. Obstacles with a height of h and a width of $w = 0.5$ cm are evenly spaced with 8 cm along the length of the channel and attached to the top and bottom channel walls. The channel is filled with stoichiometric hydrogen-air mixture at 1 atm, and 293 K with parameters defined in Table I. Initially, a small pocket of burned area (red area in Fig. 3) is used to ignite the mixture. The minimum cell size is $dx_{\min} = 1/256$ cm, where Gamezo et al. [16] showed using a similar computational setup to be sufficient to resolve the flames and shocks and achieve grid independence for the onset of detonations. Earlier work by Goodwin et al. [36] shows that the detonation mechanisms in an obstructed channel are largely affected by the channel blockage ratio (br). In the following section, a blockage ratio, $br = 2h/D$ of 0.5 is carefully selected such that both ignition mechanisms: hot spot ignited in a gradient of reactivity, and shock-focusing in an energetic gas are found.

The evolution of the flame in an obstructed channel has been studied and documented in a number of prior works for different fuels-oxidizer mixtures [16,26,36,38]. The flame acceleration

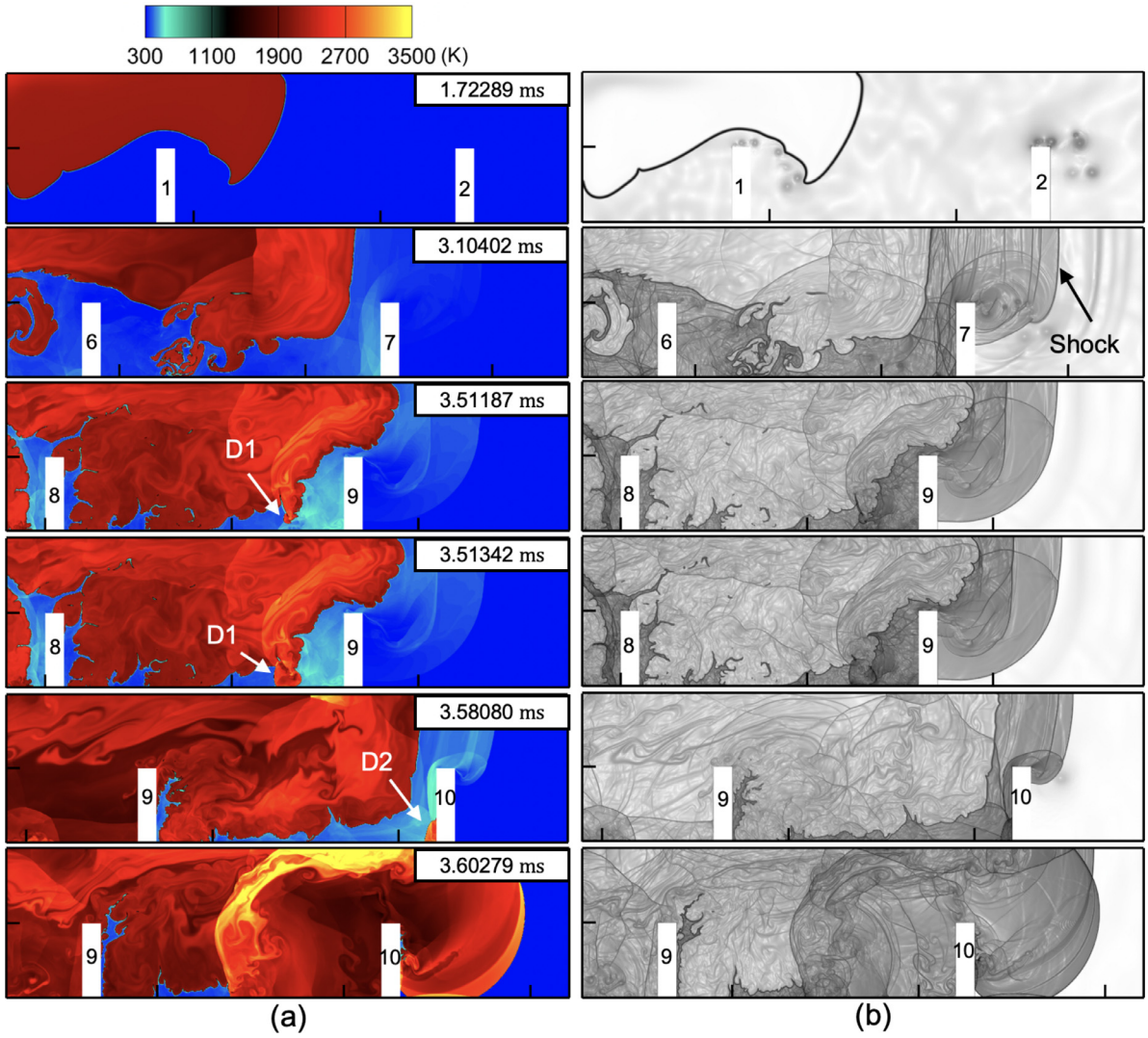

Fig. 4. Sequence of (a) temperature fields and (b) corresponding numerical schlieren fields showing the flame acceleration and detonation ignition for hydrogen-air mixture in an obstructed channel with $br = 0.5$. Detonations D1 and D2 are labeled.

in the hydrogen-air mixture follows a similar trend and the simulation result is shown in Fig. 4. Initially, the laminar flame accelerates as it expands over the obstacles, pushing the unreacted material along the channel. The flame surface area keeps increasing as it passes the obstacles due to primarily Rayleigh-Taylor and Richtmyer-Meshkov instabilities. As the flame becomes fast enough, a strong shock (marked in the second frame of Fig. 4) forms ahead of the flame front, and the flame is continuously distorted through shock-flame interactions. Here, the flame velocity is typically from 1/3 to 1/2 of the CJ detonation speed (D_{CJ}), which corresponds to the 40% D_{CJ} deflagration case shown in the 1D section.

Transition to detonation occurs as the shock collisions raise the temperature and pressure behind the leading shock wave, and the reaction is triggered in the unburned area directly by shock compression. The onset of detonation ignitions is shown in frames 3 to 6 of Fig. 4. Here, two detonation initiations through different mechanisms are observed, making this configuration a particularly interesting case. The first ignition occurs at about 3.51 ms ("D1" in Fig. 4) as multiple shock waves reflected from the obstacles and the bottom wall collide on the flame surface, causing the flame front to transition to a detonation directly. This process corresponds to shock-focusing, which could be related to either the reactivity-gradient mechanism or the direct initiation mechanism. However, the first detonation fails possibly due to the insufficient unburned materials for the detonation wave to propagate. A second ignition ("D2" in Fig. 4) is induced by a hot spot at the corner of the next obstacle (#10) due to shock collisions at around 3.58 ms. This second ignition from a hot spot, typically related to the reactivity-gradient mechanism, succeeds in transitioning into a detonation wave.

Conventional diagnostics such as shown in Fig. 4 are traditionally used for numerical investigation of the DDT process. Typically, numerical schlieren, pressure, and temperature fields can successfully capture the flame behavior and the flow features. Post-processed variables such as shock velocity, flame velocity, energy release rate, etc. are often calculated to further investigate the detonation physics. These conventional diagnostics allow for both quantification and visualization of the flame and flow behavior. The analysis leads to a general consensus that the detonation ignition occurs as a consequence of shock reflections and compression. Beyond this, however, the fundamental physics of each mechanism, especially the combustion features as well as the role of shock-induced compressibility to the detonation initiations are still unclear. The CEMA methodology, described in Section 2.4, can provide new insights into understanding different detonation ignition modes by quantifying the relative importance of chemical reaction, diffusion, and compressibility.

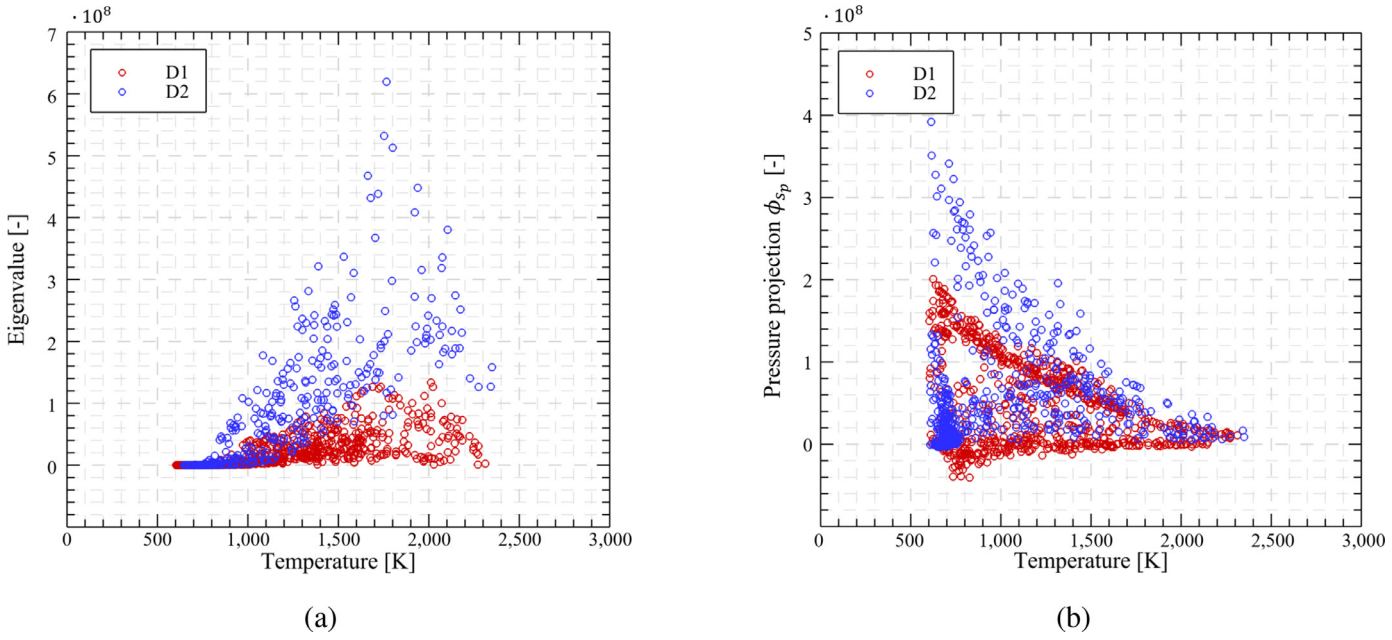

Fig. 5. Scatter plots showing the distribution of (a) temperature and eigenvalue λ_e; (b) temperature and ϕ_{s_p} of the CEM around detonation points D1 and D2 in the channel.

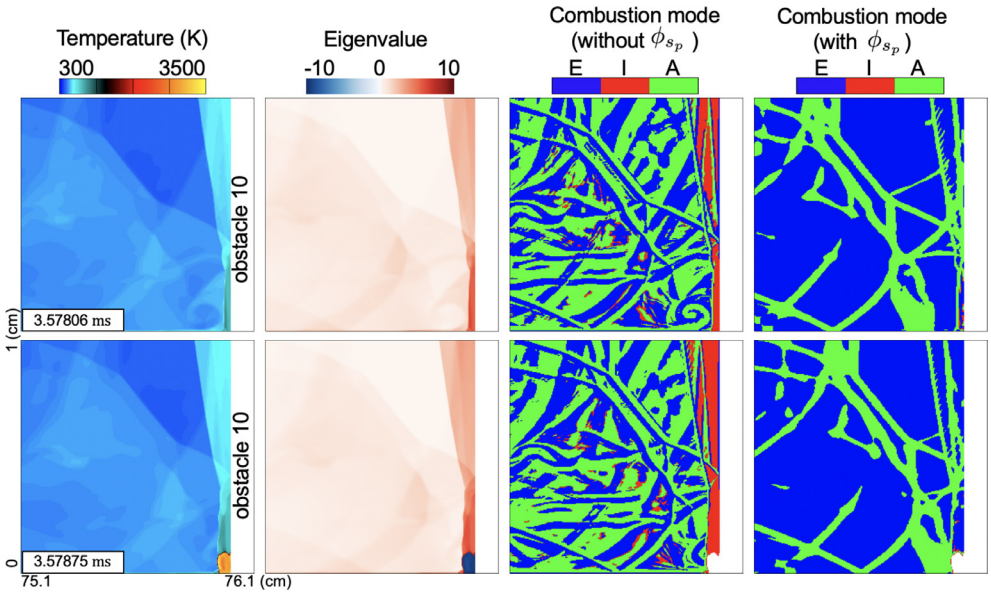

Fig. 6. Computed isocontours of temperature, CEM eigenvalue, local combustion modes without/with the contribution from compressibility (ϕ_{s_p}) before/after the second detonation point (D2). The eigenvalue fields are calculated as $\text{sign}(\lambda_e) \times \log_{10}(1 + |\lambda_e|)$. Colors on the combustion mode plots indicate the auto-ignition (red, "I"), assisted-ignition (green, "A") and local extinction (blue, "E") modes, respectively. (For interpretation of the references to colour in this figure legend, the reader is referred to the web version of this article.)

The CEMA-based criteria are employed in the simulation results, and the contours of temperature, the CEM eigenvalue (λ_e), and the local combustion modes near the two ignition spots ("D2" and "D1" marked in Fig. 4) are shown in Fig. 6 and 7. Both combustion modes without and with the consideration of ϕ_{s_p} are presented as a comparison. The criterion used to identify the auto-ignition mode, the assisted-ignition mode, and the extinction mode is consistent with the work by Xu et al. [21] and is described in detail in Section 2D. For the case without ϕ_{s_p}, the combustion mode indicator is defined as

$$\alpha = \frac{\phi_{s_d}}{\phi_\omega} \tag{30}$$

where only the relative importance of chemistry and diffusion are considered and the term ϕ_{s_p} is omitted. When including the contribution of pressure-induced compressibility, the newly defined combustion mode indicator, α^*, reads,

$$\alpha^* = \frac{\phi_{s_d} + \phi_{s_p}}{\phi_\omega} \tag{31}$$

Within this definition, α^* can highlight the relative importance of chemical, diffusive, and compressibility contribution to the CEM in compressible flows where the ignition modes can be defined as (i) $\alpha^* > 1$: the assisted-ignition mode, where diffusion and pressure-induced compressibility dominates chemistry and promotes ignition; (ii) $|\alpha^*| < 1$: the auto-ignition mode, where chemistry plays a dominant role in the ignition with diffusion and compressibility being less important; (iii) $\alpha^* < -1$: the local extinction mode, where diffusion and compressibility dominate chemistry but reverses the ignition process.

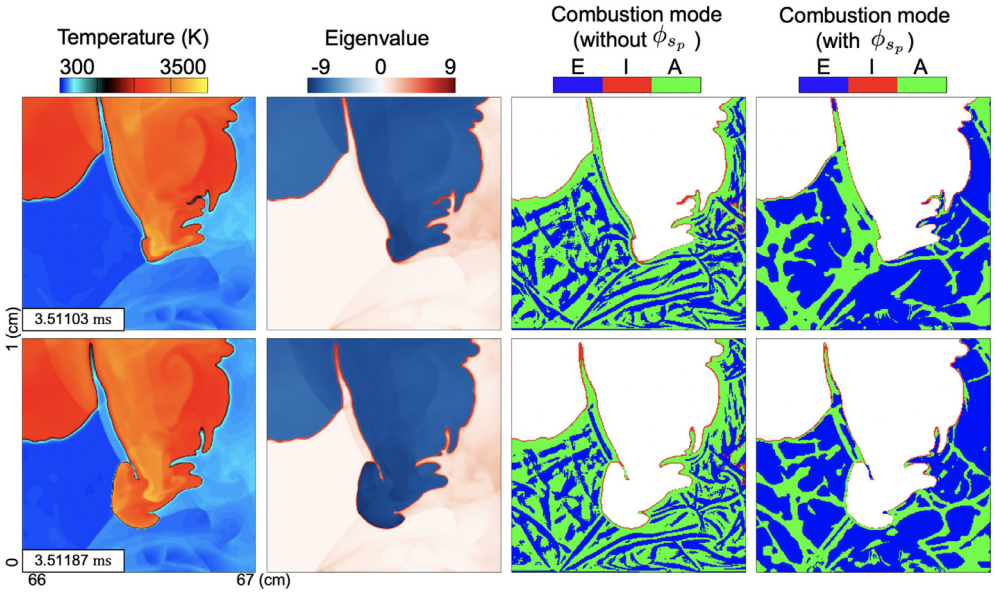

Fig. 7. Computed isocontours of temperature, CEM eigenvalue, local combustion modes without and with the contribution from compressibility (ϕ_{s_p}) before and after the first detonation point (D1). The eigenvalue fields are calculated as $\text{sign}(\lambda_e) \times \log_{10}(1 + |\lambda_e|)$.

In order to review the detonation initiation mechanisms of the two highlighted spots ("D2" and "D1"), the relation between the eigenvalues of the CEM (λ_e) and the temperatures at local regions of these two spots shortly after the detonation ignition is examined in Fig. 5(a). While both spots achieved autoignition indicated by the highly positive value of the eigenvalue at high temperatures, at ignition onset, the eigenvalues achieved near detonation point "D2" is found to be significantly higher than that of "D1". The result indicates that the detonation development is manifested by the high eigenvalue of CEM prior to the event. The significantly lower value of eigenvalues near "D1" can be seen as an indication of why the detonation was not sustained further. Accordingly, the pressure-induced compressibility contributions to the CEM are depicted in Fig. 5(b). As expected the compressibility contribution happens at a much lower temperature possibly corresponding to non-reacting flows ahead of the flame in "D1" and regions near the obstacles in "D2". The magnitude of the pressure contribution is also comparable compared to the eigenvalue which indicates the importance of pressure contribution in the process of deflagration to detonation transition. This is intuitive as detonation can be seen as a result of the positive feedback between the heat release in the ignition front and the pressure wave [19]. This further demonstrates the importance of including pressure-induced compressibility in the budget analysis of CEM. With the inclusion of compressibility in the new combustion mode $|\alpha^*|$, more in-depth analysis can be performed to study the details of detonation initiation between these two spots.

The above-mentioned CEMA-based analysis near detonation point "D2", which later on successively transits into a detonation is presented in Fig. 6. Here, the leading shock wave reflects from the obstacle and the bottom channel wall, forming Mach stems. A region with an extreme positive λ_e is observed at the corner of obstacle #10 at 3.57806 ms. This highly reactive region suggests a possible detonation reignition within this area. In fact, a hot spot ignites near the local maximum λ_e at around $t = 3.57875$ ms. The local combustion mode analysis presented in Fig. 6 shows that the hot-spot induced reignition is mainly driven by the auto-ignition mode (red region) where diffusion and compressibility play a negligible role. Using the previous CEMA criterion (without ϕ_{s_p}), a large region of auto-ignition mode is observed behind the reflected Mach stem. This is intuitive as the original combustion mode only compares the diffusion and autoignition contribution in a CEM. While diffusion can play a significant role in various flames as indicated by previous studies using such criteria [21], diffusion can be significantly less important in the DDT process as suggested by previous studies [3]. Therefore, the comparison of only diffusion and autoignition can be erroneous in identifying the underlying mechanisms of detonations. This is indeed shown in Fig. 6, when including the effect of compressibility (last column), only a very small region featuring auto-ignition mode is found at the corner. This is likely due to the positive contribution of ϕ_{s_p} to the combustion mode indicator through shock wave compression from the Mach stem-obstacle collisions. This result is consistent with the previous finding that the reactivity gradient, which is essential for a hot-spot-induced detonation, comes from shock compression, instead of turbulent mixing of the reacted and unreacted materials [16]. In addition, the region of local extinction mode (blue region) becomes larger when including the effect of compressibility. This can be associated with the pressure wave locally expanding to lower pressures, and therefore leading to a lower state of energy prohibiting the detonation propagation/initiation in this region. In general, the new CEMA criterion has worked as a much more accurate precursor in identifying the detonation onset.

Perhaps what is more interesting, in this case, is the first detonation ("D1" marked in Fig. 4) that is initiated by multiple shocks colliding on the flame front. This so-called "shock-focusing" mechanism is one of the primary mechanisms for DDT occurrence in the obstructed channels, where the pressure-induced compressibility is considered to be critical. Figure 7 shows the temperature, eigenvalue, and local combustion mode contours near the first detonation spot. At $t = 3.51103$ ms, multiple shock waves collide on the flame front, leaving a small region of large positive λ_e behind. At $t = 3.51187$ ms, a detonation is initiated at the colliding point. Similarly, the auto-ignition mode is observed near the detonation spot, suggesting that local chemistry plays a predominant role. In the surrounding area of the ignited kernel, both assisted-ignition mode and local extinction mode are present. Comparing results from the last two columns of Fig. 7, a larger area of extinction mode is observed when taking into account the ϕ_{s_p} term. This suggests that pressure-induced compressibility could inhibit the ignition process. In addition, at $t = 3.51103$ ms, the assisted-ignition mode dominates on one side of the flame, while extinction mode dominates

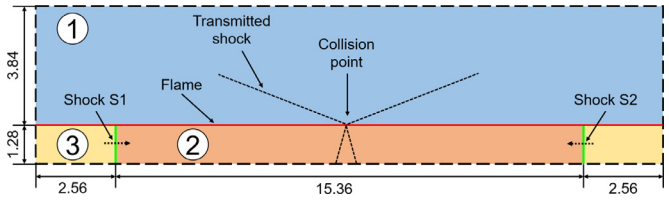

Fig. 8. Schematic of an idealized physical model for analysing shock-focusing induced detonation initiation. Units are millimeters. Incident shocks and flame surfaces are colored green and red, respectively. (For interpretation of the references to colour in this figure legend, the reader is referred to the web version of this article.)

on the other side. As a result, the flame has a propensity of propagating in the direction towards the assisted-ignition region where limited reactive gas is available to sustain the detonation propagation. While in this case, the proposed criteria can serve as an unambiguous marker for the resultant explosive dynamics, scarce information on the detonation initiation mechanisms relevant to the shock-focusing mechanism can be extracted due to the limited grid resolution at the flame and shock fronts. As suggested by Xiao et al. [4], detonations at the flame front could be initiated by either a reactivity-gradient mechanism or a direct initiation mechanism all accompanied by shock-focusing. Therefore, for the channel case presented here, a more detailed analysis regarding each initiation mechanism for shock-focusing at the flame front is needed to validate the proposed CEMA criteria. Simulation results on idealized configurations are provided in the following section to further examine the shock-focusing at the flame front in detail.

3.3. An idealized model of shock-focusing

Following the same configurations for shock focusing at the flame front proposed by Xiao et al. [4], an idealized case illustrated in Fig. 8 is investigated. Here, the computational domain consists of a burned region at the bottom and an unburned region at the top. Two incident shock waves propagate towards each other with the same Mach number, colliding on the flame front. This configuration is designed to study the ignition process similar to conditions shown in Fig. 7 while excluding excessive disturbances from the multiple shock waves for easier analysis. Therefore, the physical conditions in the initial setup are set to correspond to the state variables of the unburned and burned gases around "D1" in Fig. 4. Temperatures in the burned and unburned regions are set to be 400 and 2500 K, respectively, and the initial pressure is 11 atm. Maximum and minimum cell sizes are $d_{\max} = 40$ μm and $d_{\min} = 0.625$ μm, which corresponds to approximately 41 grid points in a laminar flame thickness. Calculations with shock waves at Mach numbers of 2.6 and 3.0 are tested to capture both the reactivity-gradient mechanism and the direct initiation mechanism.

Figure 9 shows the temperature and schlieren fields at selected times illustrating the DDT process induced by focusing two shock waves with the same Mach number $M_s = 2.6$. As the two shock waves propagate towards each other, secondary shocks are generated into the unburned area while expansion waves propagate downwards (see Fig. 9 at 1.9653 μs). At 3.0353 μs, the two shock waves collide with each other. Transmitted shocks and reflected shocks are found as a result of the interactions between the shocks and the interface. After the collision, the shocks carry the flame in the vertical direction, forming a mushroom-shaped flame structure 3.9081 μs. The mushroom-like flame grows in the unburned region, forming a strong leading shock ahead of the flame. Later, two detonation points (indicated by "D" in the last frame of Fig. 9) are found near the slip lines at 4.0814 μs. In addition, the idealized configuration with stronger shock waves, $M_s = 3.0$, is examined and the detonation ignition process is shown in Fig. 10. Unlike the case with $M_s = 2.6$, where there is a delayed transition to detonation, here, the two incident shocks collide on the flame front at about 2.5540 μs, and a detonation initiates almost immediately after the collision. These distinct behaviors are likely due to the fundamental physics underlying the two detonation ignition mechanisms and merit further investigation.

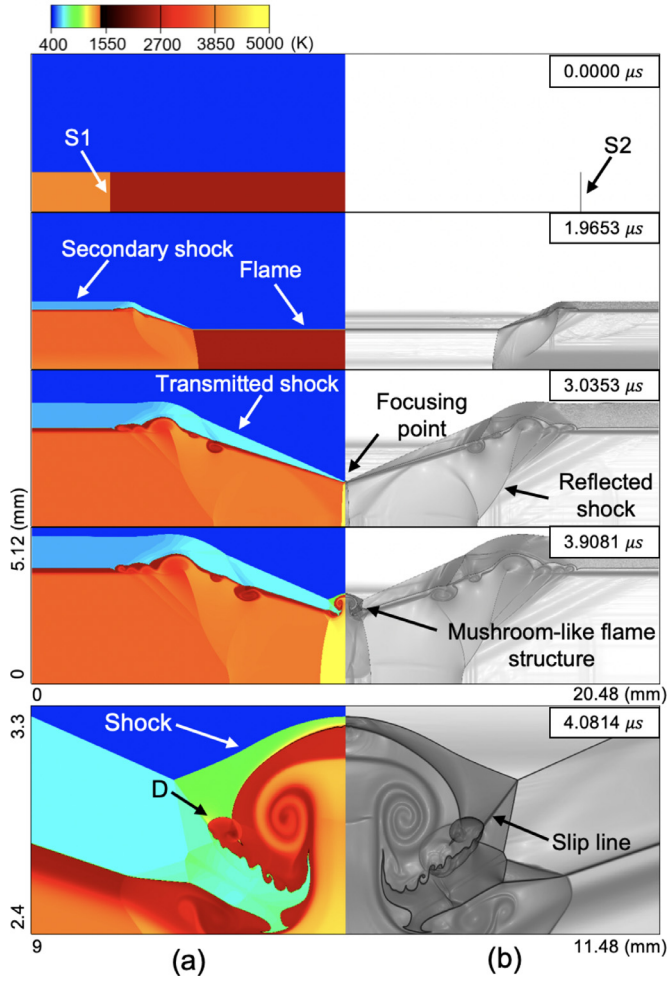

Fig. 9. Time sequence of (a) temperature fields (left half of the domain) and (b) corresponding schlieren fields (right half) showing shock focusing and detonation by two propagating shock waves with Mach number $M_s = 2.6$.

Figures 11 and 12 show the temperature fields and CEMA combustion mode analysis in a small DDT region before and after the detonation ignition for the two test cases. For the case of $M_s = 2.6$, a gradient of temperature is found in front of the flame at the slip line (see temperature contour at 4.03778 μs in Fig. 11), inducing a spontaneous wave that soon develops into an overdriven detonation. Here, the detonation is ignited through the Zeldovich gradient mechanism, where a gradient of reactivity or temperature is essential [6,39]. This gradient mechanism can be verified through the distribution of eigenvalue λ_e, and local combustion modes. As shown, a highly reactive region is formed between the leading shock wave and the slip line. The detonation initiates at the location of the maximum λ_e, which corresponds to the local minimum chemical induction time. In addition, from the last frame of Fig. 11 at 4.03778 μs, there is a small region where all three combustion modes (auto-ignition, assisted-ignition, and extinction) coexist at the flame front, resulting in an obvious reactivity gradient. This is because the compression waves generated by the spontaneous wave lead to a localized pressure increase ahead of

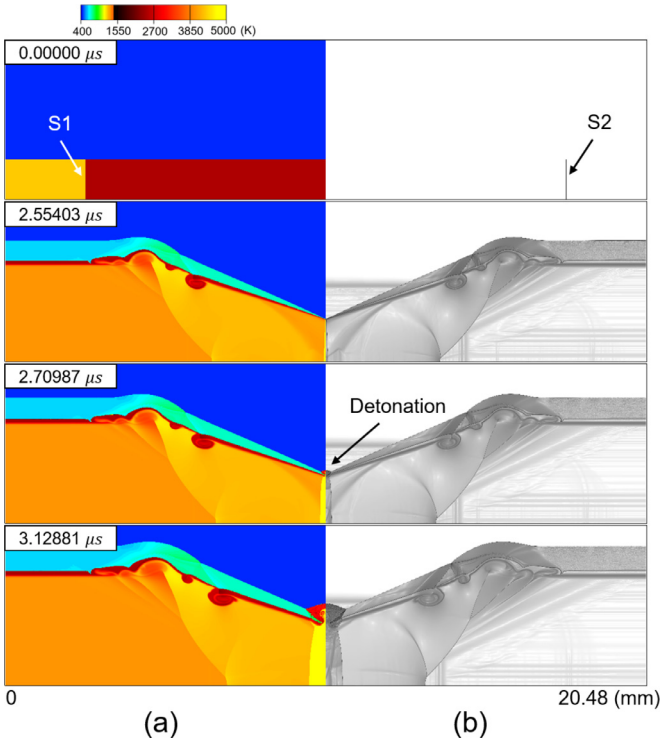

Fig. 10. Time sequence of (a) temperature fields (left half of the domain) and (b) corresponding schlieren fields (right half) showing shock focusing and detonation by two propagating shock waves with Mach number $M_s = 3.0$.

the flame tip. The compression leads to in a positive contribution of the ϕ_{s_p} term, raising the value of α^* to the range of assisted-ignition mode at the flame front. In addition, a region dominated by the auto-ignition mode (red) and a region dominant by the extinction mode (blue) is separated by the slip line. This suggests that the detonation spot, once ignited, propagates toward the upper side of the slip line which corresponds well to previous findings that detonations will first sweep towards the higher temperature region and then propagates across the slip line, eventually propagates into lower temperature regions [4]. The prediction of flame propagation propensity is further confirmed by the solution shown at $t = 4.06393$ μs. Moreover, using the current CEMA formulation, the detonation onset is clearly demonstrated as a consequence of the shock-to-shock interactions where detonation can be seen as a result of the positive feedback between the heat release through chemistry and the pressure wave. Such a finding is consistent with recent studies where a stronger pressure wave is found to increase the role of transport that enhances the subsequent detonation development [19,40,41]. Such characteristics, however, are not captured with the previous CEMA criterion (third column in Fig. 11). Therefore, the results demonstrated in this study suggest that taking into account the contribution of pressure-induced compressibility to CEM is essential for analyzing the shock-focusing mechanism.

As a comparison, the CEMA analysis is applied to the DDT region for the case of $M_s = 3.0$, where ignition occurs directly after the shock collision (see Fig. 12). During this process, a highly reactive region is formed between the flame and the transmitted shock wave. The strong incident shock waves compress the material near the colliding point, where only the assisted-ignition mode (green region) is observed at $t = 2.53500$ μs using the new CEMA criterion. Here, the assisted ignition primarily driven by the pressure compression leads to a direct detonation initiation. On both sides of the colliding point, however, there is again a reactivity gradient similar to the case discussed above.

To further quantify the reactivity and the effect of pressure-induced compressibility on the two mechanisms, Fig. 13 (a) and (b) highlight the eigenvalue and the pressure-induced compressibility contribution to the CEM for the two cases. From Fig. 13 (a), the highest eigenvalue obtained by the two idealized cases after the detonation is comparable to that obtained in "D2" (see Fig. 5(a)) where successful detonation is formed. The distribution of eigenvalues for the two cases has similar shapes. However, the case of $M_s = 2.6$ has a much wider span of eigenvalues across the temperature range compared to the case of $M_s = 3.0$. In addition, Fig. 13 (b) suggests that for the stronger case ($M_s = 3.0$), the compressibility contribution is significantly greater than that of the weaker case ($M_s = 2.6$). These results correspond well with the physical interpretation given by Xiao et al. [4] that two mech-

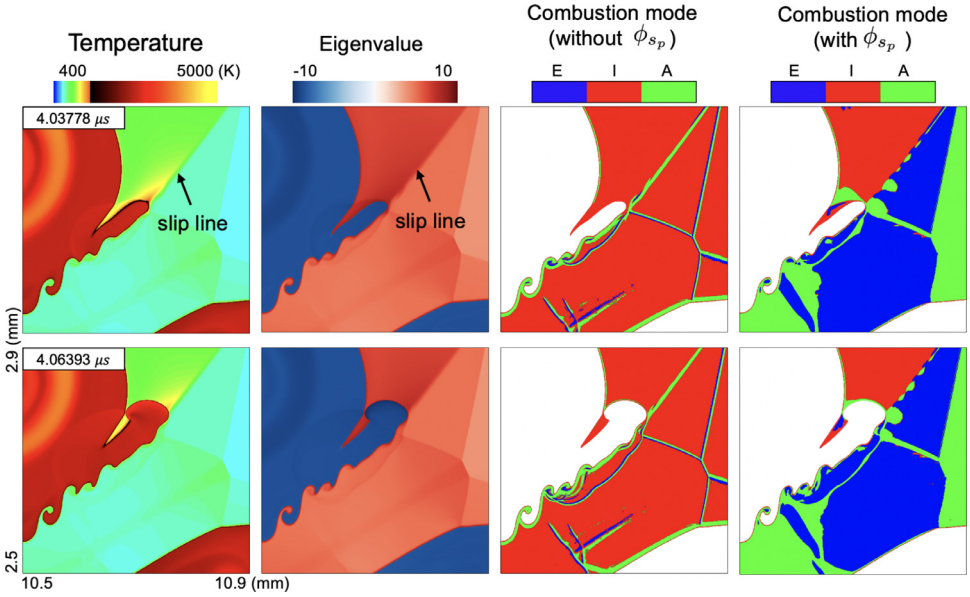

Fig. 11. Isocontours of temperature, CEM eigenvalue, local combustion modes with and without the contribution from compressibility (ϕ_{s_p}) in the DDT region before and after the detonation ignition for the case of $M_s = 2.6$.

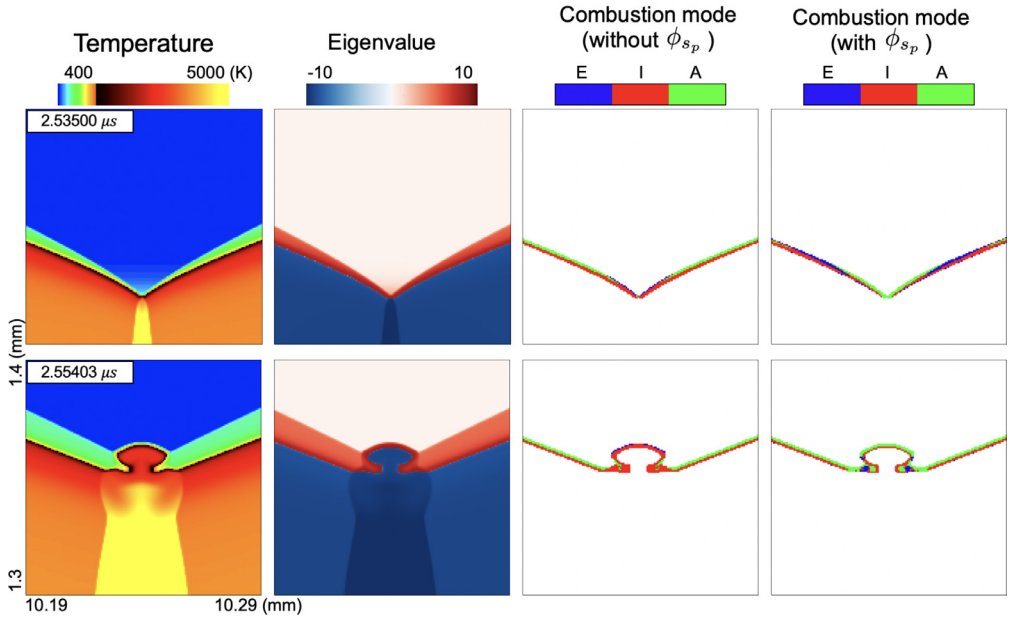

Fig. 12. Isocontours of temperature, CEM eigenvalue, local combustion modes with and without the contribution from compressibility (ϕ_{s_p}) in the DDT region before and after the detonation ignition for the case of $M_s = 3.0$.

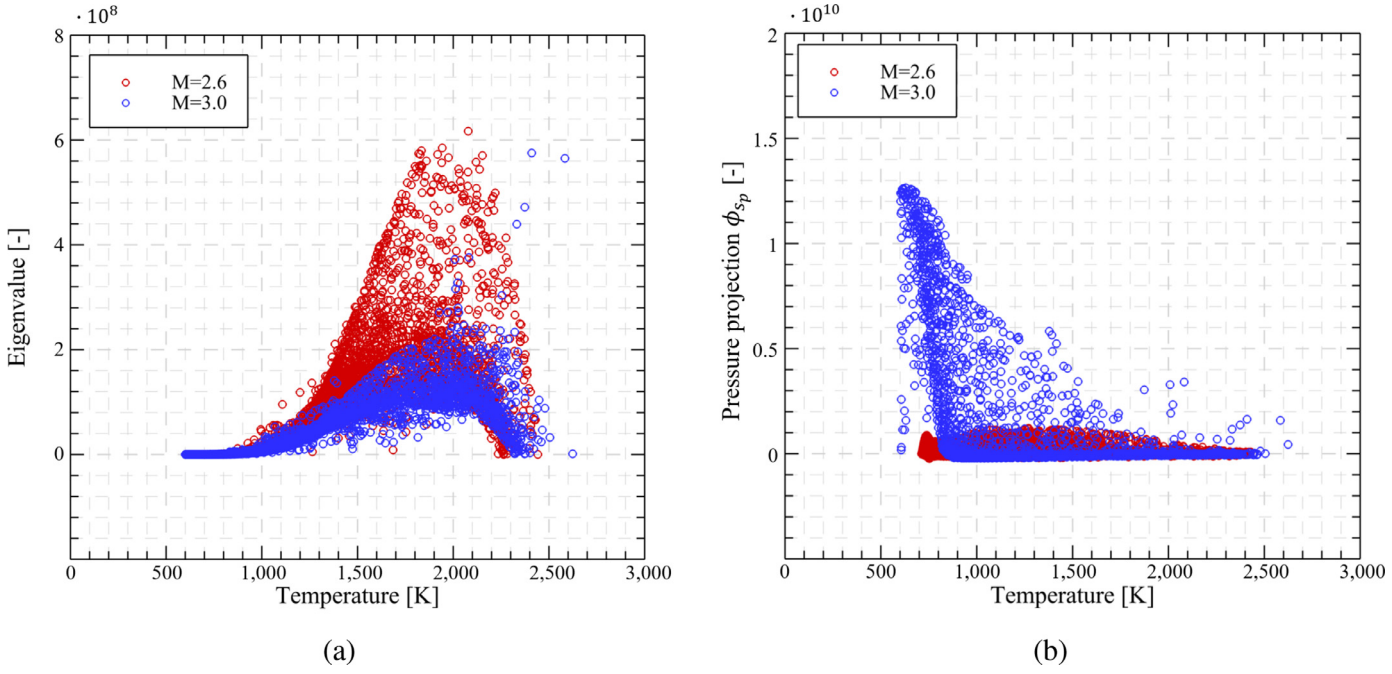

Fig. 13. Scatter plots showing the distribution of (a) temperature and eigenvalue λ_e; (b) temperature and ϕ_{s_p} of the CEM around detonation points in idealized case with $M_s = 2.6$ and $M_s = 3.0$.

anisms of detonation formation might exist at the flame front where one refers to focusing of relatively weak shocks leading to a delayed transition to detonation through the reactivity-gradient mechanism ($M_s = 2.6$) and the other refers to direct detonation initiation ($M_s = 3.0$) triggered at the collision spot by focusing shocks at the flame front. The wider λ_e distribution for the $M_s = 2.6$ case suggests a greater reactivity gradient near the detonation spot, which is the key element for a reactivity-gradient mechanism. For the case of $M_s = 3.0$, however, the smaller eigenvalue span suggests a small reactivity gradient which could be insufficient to induce a spontaneous wave for the detonation. Note that despite the lower eigenvalue distribution, a few points of high λ_e value exist for the $M_s = 3.0$ case. The scarce points of $M_s = 3.0$ can also be interpreted as the shock collision deposits energy in a localized spot where the timescale of energy deposit is much smaller compared to the acoustic timescale of the gas resulting in a direct initiation. In summary, the new CEMA works successively in capturing the process of shock-focusing and identifying the corresponding detonation ignition mechanism (autoignition-supported gradient mechanism or direct ignition mechanism).

4. Summary and conclusions

This paper presents a new flame diagnostic method for the compressibility effects in the chemical explosive mode analysis

(CEMA) framework during the deflagration to detonation transition (DDT) process, where the compressible reactive flow involving shocks and turbulence is considered. The new formulation introduces the effect of pressure-induced compressibility in CEMA, and the relevant contributions of chemical reaction, diffusion, and compressibility are compared with each other to identify the local combustion modes during the DDT process. The numerical model solves the compressible reactive Navier-Stokes equations by a high-order Godunov algorithm on an adapting grid. A single-step, calibrated chemical-diffusive model of the Arrhenius form is used for the reaction of stoichiometric hydrogen-air mixture.

First, the new formulation has been validated through a series of 1D premixed hydrogen-air flame configurations: laminar flame propagation, post-shock laminar flame, and the Chapman-Jouguet detonation. For the laminar flame and post-shock laminar flame, chemistry dominates at higher temperatures and diffusion dominates at the lower temperature. No compressibility contribution can be found. For the CJ detonation case, however, a switchover between compressibility and diffusion is observed in the induction zone, which then leads to an auto-ignition in the reaction zone. The 1D results show that the new CEMA projection formulation is able to capture the key contributions of chemical and nonchemical terms in the main scenarios involved in DDT, and can clearly distinguish between deflagration and shock-induced detonation.

Then, multi-dimensional, unsteady simulations of an obstructed channel filled with a stoichiometric hydrogen-air mixture are performed with a particular interest in CEMA diagnostics for different detonation ignition modes. For the case of blockage ratio $br = 0.5$, two detonation points are found, one is ignited through shock focusing on the flame front, and the other one through a hot spot at the corner of the obstacle. The CEMA analysis shows that both of the two detonation processes are well captured, where detonation initiations are featured by a highly-reactive region and the local auto-ignition mode. Comparison between the newly proposed and the previous CEMA projection formulations shows that involving the contribution of compressibility leads to a more accurate identification of the detonation onset region, and thus pressure-induced compressibility is essential for CEMA in DDT. Following the channel flow case, an idealized configuration of focusing two shock waves with $M_s = 2.6$ and 3.0 are tested to investigate the detailed shock focusing mechanism with increased mesh resolution. The results show that the current CEMA projection formulation can well identify the gradient mechanism and the direct initiation mechanism. For the gradient-induced mechanism, an apparent reactivity gradient featuring all three CEM modes is present in front of the flame and the propensity of the flame propagation is correctly captured. For the case of focusing two stronger shocks, a considerably smaller eigenvalue span, and greater compressibility contribution have been observed, which suggests that the detonation is ignited through a direct initiation mechanism. Using the current CEMA projection formulation, the detonation onset is clearly demonstrated as a consequence of the shock-to-shock interactions where detonation can be seen as a result of the positive feedback between the heat release through chemistry and the pressure wave. The role of compressibility is also found enhanced at the edge of the detonation front where diffusion was found to have minimal effects on detonation development.

Declaration of Competing Interest

The authors declare that they have no known competing financial interests or personal relationships that could have appeared to influence the work reported in this paper.

CRediT authorship contribution statement

S. Lai: Conceptualization, Formal analysis, Writing – original draft, Writing – review & editing, Funding acquisition, Supervision. **S. Tang:** Investigation, Data curation, Writing – original draft, Writing – review & editing. **C. Xu:** Conceptualization, Methodology, Investigation, Writing – review & editing. **N. Sekularac:** Investigation, Writing – review & editing. **X. Fang:** Conceptualization, Methodology, Formal analysis, Writing – original draft, Writing – review & editing, Supervision, Funding acquisition.

Acknowledgments

This study was supported by the National Natural Science Foundation of China (Grant No. 12002207) and Shanghai Pujiang Program (20PJ408500). All the computations were carried out on SJTU supercomputing resources (https://hpc.sjtu.edu.cn/). Dr. XiaoHang Fang gratefully acknowledges the financial support from the John Fell Oxford University Press Research Fund (0011348) and the VPR Catalyst Grant (10040436) from the University of Calgary. The authors are particularly grateful to Professor Elaine Oran for developing and sharing the computing code for DDT simulations.

References

[1] P. Senecal, F. Leach, Diversity in transportation: why a mix of propulsion technologies is the way forward for the future fleet, Result. Eng. 4 (2019) 100060.
[2] Y. Gao, P. Dai, Z. Chen, Numerical studies on autoignition and detonation development from a hot spot in hydrogen/air mixtures, Combust. Theor. Model. 24 (2020) 245–261.
[3] S. Lai, C. Xu, M. Davy, X. Fang, Flame acceleration and transition to detonation in a pre-/main-chamber combustion system, Phys. Fluids 34 (2022) 116105.
[4] H. Xiao, E.S. Oran, Shock focusing and detonation initiation at a flame front, Combust. Flame 203 (2019) 397–406.
[5] W. Han, W. Ma, C. Qian, J. Wen, C. Wang, Bifurcation of pulsation instability in one-dimensional $H_2 - O_2$ detonation with detailed reaction mechanism, Phys. Rev. Fluids 4 (2019) 103202, doi:10.1103/PhysRevFluids.4.103202.
[6] E.S. Oran, V.N. Gamezo, Origins of the deflagration-to-detonation transition in gas-phase combustion, Combust. Flame 148 (2007) 4–47.
[7] M. Zhao, M.J. Cleary, H. Zhang, Combustion mode and wave multiplicity in rotating detonative combustion with separate reactant injection, Combust. Flame 225 (2021) 291–304.
[8] R. Zhu, X. Fang, C. Xu, M. Zhao, H. Zhang, M. Davy, Pulsating one-dimensional detonation in ammonia-hydrogen-air mixtures, Int. J. Hydrogen Energy 47 (2022) 21517–21536.
[9] K.N.C. Bray, N. Nikiforakis, J.H.S. Lee, A.J. Higgins, Comments on criteria for direct initiation of detonation, Philos. Trans. R. Soc. Lond. Ser. A: Math. Phys. Eng. Sci. 357 (1764) (1999) 3503–3521.
[10] M. Liberman, M. Ivanov, A. Kiverin, M. Kuznetsov, A. Chukalovsky, T. Rakhimova, Deflagration-to-detonation transition in highly reactive combustible mixtures, Acta Astronaut. 67 (7) (2010) 688–701.
[11] A.D. Kiverin, D.R. Kassoy, M.F. Ivanov, M.A. Liberman, Mechanisms of ignition by transient energy deposition: regimes of combustion wave propagation, Phys. Rev. E 87 (2013) 033015.
[12] C. Qi, Z. Chen, Effects of temperature perturbation on direct detonation initiation, Proc. Combust. Inst. 36 (2017) 2743–2751. https://www.sciencedirect.com/science/article/pii/S1540748916301511.
[13] Y. Zel'dovich, V. Librovich, G. Makhviladze, G. Sivashinsky, On the development of detonation in a non-uniformly preheated gas, Astronautica Acta 15(1970) 313–321. https://www.scopus.com/inward/record.uri?eid=2-s2.0-0001609020&partnerID=40&md5=e1fcb18c0c3bb54172d7c8d1b17093a2.
[14] J. Lee, R. Knystautas, N. Yoshikawa, Photochemical initiation of gaseous detonations, Acta Astronaut. 5 (1978) 971–982.
[15] P. Strakey, D. Ferguson, A. Sisler, A. Nix, Computationally quantifying loss mechanisms in a rotating detonation engine (????).
[16] V.N. Gamezo, T. Ogawa, E.S. Oran, Numerical simulations of flame propagation and ddt in obstructed channels filled with hydrogen–air mixture, Proc. Combust. Inst. 31 (2007) 2463–2471.
[17] R.X. Zhu, S. Tang, S. Lai, X. Fang, M. Davy, C. Xu, Parametric studies of deflagration-to-detonation transition in a pre-chamber/main-chamber system, ASME 2022 ICE Forward Conf. (2022).
[18] D.A. Goussis, H.G. Im, H.N. Najm, S. Paolucci, M. Valorani, The origin of cema and its relation to csp, Combust. Flame 227 (2021) 396–401.
[19] I. D. Dimitrova, S. Sanal, M.B. Luong, E. Tingas, H. Im, Asymptotic analysis of detonation development at si engine conditions using computational singular perturbation(2022). doi:10.20944/preprints202205.0377.v1.
[20] T.F. Lu, C.S. Yoo, J.H. Chen, C.K. Law, Three-dimensional direct numerical simulation of a turbulent lifted hydrogen jet flame in heated coflow: a chemical explosive mode analysis, J. Fluid Mech 652 (2010) 45–64.

[21] C. Xu, J.-W. Park, C.S. Yoo, J.H. Chen, T. Lu, Identification of premixed flame propagation modes using chemical explosive mode analysis, Proc. Combust. Inst. (2019).
[22] C. Xu, A.Y. Poludnenko, X. Zhao, H. Wang, T. Lu, Structure of strongly turbulent premixed n-dodecane-air flames: direct numerical simulations and chemical explosive mode analysis, Combust. Flame 209 (2019) 27–40.
[23] W. Xie, W. Wu, Z. Ren, H. Liu, M. Ihme, Effects of evaporation on chemical reactions in counterflow spray flames, Phys. Fluids 33 (2021).
[24] T. Jaravel, O. Dounia, Q. Malé, O. Vermorel, Deflagration to detonation transition in fast flames and tracking with chemical explosive mode analysis, Proc. Combust. Inst. 38 (2021) 3529–3536.
[25] W. Wu, Y. Piao, Q. Xie, Z. Ren, Flame diagnostics with a conservative representation of chemical explosive mode analysis, AIAA J. 57 (2019) 1355–1363.
[26] V.N. Gamezo, T. Ogawa, E.S. Oran, Flame acceleration and ddt in channels with obstacles: effect of obstacle spacing, Combust. Flame 155 (2008) 302–315. https://www.sciencedirect.com/science/article/pii/S0010218008001934
[27] X. Lu, C.R. Kaplan, E.S. Oran, A chemical-diffusive model for simulating detonative combustion with constrained detonation cell sizes, Combust. Flame 230 (2021) 111417.
[28] M. Li, D. Liu, T. Shen, J. Sun, H. Xiao, Effects of obstacle layout and blockage ratio on flame acceleration and ddt in hydrogen-air mixture in a channel with an array of obstacles, Int. J. Hydrogen Energy 47 (8) (2022) 5650–5662.
[29] L. Shi, K.C.K. Uy, C.Y. Wen, The re-initiation mechanism of detonation diffraction in a weakly unstable gaseous mixture, J. Fluid Mech. 895 (2020) A24, doi:10.1017/jfm.2020.311.
[30] M. Peswani, B. Maxwell, Detonation wave diffraction in stoichiometric c2h4/o2 mixtures using a global four-step combustion model, Phys. Fluids 34 (2022) 106104.
[31] J. Bell, A. Almgren, V. Beckner, M. Day, M. Lijewski, A. Nonaka, W. Zhang, Boxlib user guide, github. com/BoxLib-Codes/BoxLib (2012).
[32] W. Zhang, A. Almgren, M. Day, T. Nguyen, J. Shalf, D. Unat, Boxlib with tiling: an adaptive mesh refinement software framework, SIAM J. Sci. Comput. 38 (2016) S156–S172.
[33] J.H.S. Lee, The Detonation Phenomenon, Cambridge University Press, 2008, doi:10.1017/CBO9780511754708.
[34] B. Maxwell, Turbulent combustion modelling of fast flames and detonations using compressible lem-les (2016).
[35] B. Maxwell, A. Pekalski, M. Radulescu, Modelling of the transition of a turbulent shock-flame complex to detonation using the linear eddy model, Combust. Flame 192 (2018) 340–357, doi:10.1016/j.combustflame.2018.02.013.
[36] G. Goodwin, R. Houim, E. Oran, Effect of decreasing blockage ratio on ddt in small channels with obstacles, Combust. Flame 173 (2016) 16–26.
[37] G.B. Goodwin, E.S. Oran, Premixed flame stability and transition to detonation in a supersonic combustor, Combust. Flame 197 (2018) 145–160.
[38] G. Goodwin, R. Houim, E. Oran, Shock transition to detonation in channels with obstacles, Proc. Combust. Inst. 36 (2017) 2717–2724.
[39] Y.B. Zeldovich, On the development of detonation in a nonuniformly heated gas, Astro. Acta 15 (1970) 313–321.
[40] Q. Meng, M. Zhao, Y. Xu, L. Zhang, H. Zhang, Structure and dynamics of spray detonation in n-heptane droplet/vapor/air mixtures, Combust. Flame 249 (2023) 112603, doi:10.1016/j.combustflame.2022.112603.
[41] A. Sow, S.-M. Lau-Chapdelaine, M. Radulescu, The effect of the polytropic index γ on the structure of gaseous detonations, Proc. Combust. Inst. 38 (2021) 3633–3640, doi:10.1016/j.proci.2020.07.067.